Delft University of Technology

FACULTY OF MECHANICAL ENGINEERING

Internship Report

Surge Vessel Thermodynamics

Student Name	Student ID
Shenghao Zhang	5473322

Supervisors:

Gosse Oldenziel

Mathieu Pourquie

December 2022

Contents

1 Introduction

1.1 Surge Vessels

Surge vessels are widely used in large pipe line systems to protect the pipelines from sudden pressure changes, which can be a result of the alter of flow rate, valves opened/closed, or pump trips. A surge vessel absorbs a brief pressure rise by receiving extra water and provides extra water during a sudden pressure drop. Heat transfer of the air inside of the vessel is of crucial interest due to the fact that different heat transfer behaviors would significantly affect designed size [1]. This heat transfer process can be divided into two steps. First, air expands when water is being drained. Thus, the temperature of the air decreases below ambient temperature. During this process, the rational heat transfer (RHT) model developed by Graze [2] can be applied by assuming ideal gas law. Various heat transfer behavior can be predicted and the resulting different vessel sizes are required by prescribing different Laplace coefficients, which lies between two extremes values: 1 and 1.4, for isothermal and adiabatic vessel walls, respectively [3]. In the second step, after water level does not drop anymore, heat would be transferred through container walls from outside to inside due to the lower inner air temperature mainly through natural heat transfer until the system reaches a new equilibrium. This report performs a Large Eddy Simulation (LES) of the air flow inside when the water level is stationary with the size of the Blue Vessel in Deltares. The numerical models and iterations are carried out with StarCCM+. The results of this simulation are compared with the previous WANDA simulation and the measurement data performed on the same vessel.

Figure 1: The Blue Vessel in Deltares

1.2 Literature review

Neumann et al [4] numerically studied the steady and oscillatory convection in cylinders heated from below. Axisymmetric streamlines and temperature distribution, as well as linear Nu-Ra relation are observed at low Ra number for aspect ratio a =0.2899 (h/d) and Prandtl =1 with Boussinesq

equations. The transition to non-axisymmetric steady convection shows strong dependence on non-linear interactions, which are more significant for small Prandtl numbers (Pr=0.02). This transition is observed at higher Rayleigh numbers when having larger Pr numbers. When Pr>1, the flow patterns are found closely related with initial conditions. The transition from steady to unsteady Rayleigh-Bernard convection happen at smaller Rayleigh numbers with smaller Prandtl numbers [5].

Roshan Samuel et al [6] investigated Rayleigh-Benard convection at high Rayleigh numbers ranging from 10^6 to 10^15 through LES with novel stretched spiral vortex sub-grid model. A $64 \times 64 \times 512$ grid was chosen for a columnar box of dimension $1 \times 1 \times 10$ with Rayleigh number 10^{11}. The results obtained good agreement with the results of direct-numerical simulation(DNS) Extensive experimental data on unsteady natural convection inside of a cylinder heated from vertical wall has been done by L. B. Evans [7]. A warm and radially well-mixed boundary layer rising at the wall was observed before it turns into the core region in the center top, resulting in a gradual plug-flow sinking as heat is constantly and uniformly supplied. The results from mathematical models also show a linear vertical temperature distribution, which is essentially equal to the quasi-steady mean fluid temperature.

E. Papanicolaou et al [8] simulated the natural convection in a vertical cylinder at high Rayleigh numbers with constant heat flux through vertical wall using two-equations turbulence models. After an oscillating pattern caused by evolution of secondary flows at the core, quasi-steady state was obtained accompanied by clear temperature stratification and circular streamlines.

S.-H Peng et al [9] performed an LES of turbulent Rayleigh-Benard convection for an free-stream 6:1:6 domain at high Rayleigh numbers, showing the a single relation of Nusselt number with Rayleigh number governing the heat transfer.

1.3 Research Question

The existence of flanges and the vessel's rounded top and bottom makes the geometry complex, but its influence on heat transfer is minor. Therefore, the heat transfer problem of the Blue Vessel can be simplified as a 3-dimensional simulation of a cylinder. However, the vessel is not only heated from vertical surface, but also heated from the steel wall at the top as well as the water surface at the bottom at constant temperature. Therefore, this simulation explores the combined heat transfer phenomenon of wall-heated cylinder and Rayleigh-Benard convection. The approach to the problem can be divided into two steps: the first step deals with the validation of Rayleigh-Benard convection with small Rayleigh number, and in the second step the LES simulations of a reduced size and real size of the Blue Vessel are presented.

2 Validation: Rayleigh-Bernard convection;

2.1 Model

The simulation is started with a validation case of laminar Rayleigh-Benard convection from Neumann's work[3]. A vertical cylinder heated from below is considered. In order to obtain reasonable values for temperature differences for small Rayleigh numbers, a small dimension is assumed, with cylinder height $h = 0.01m$ and diameter $d = 0.0345m$ (aspect ratio $a = 0.2899$). Air is the Newtonian fluid inside the cylinder with prescribed constant kinematic viscosity ν, specific heat c_p, thermal conductivity k, and thermal diffusivity α. In order to match with Neumann's assumption that Prandtl number $Pr = 1$, these values are interpolated at different temperatures that slightly deviated from the mean temperature so that the adopted theoretical air properties are not too far away from reality. The air property values used are summarized in Table 1

With the largest temperature difference is lower than $15°C$, Boussinesq approximation is applied by adding a buoyancy term in the laminar momentum equations. The buoyancy term is a function of

the air density $\rho = \rho_0(1 - \beta\Delta T)$ changing linearly with temperature T, with the prescribed reference density $\rho_0 = 1.1770kg/m_3$ at reference temperature $T_0 = 300K$. The continuity, momentum, and energy equations are expressed as follows:

$$\begin{aligned} \frac{\partial u_i}{\partial x_i} &= 0 \\ \frac{\partial u_i}{\partial t} + u_j \frac{\partial u_i}{\partial x_j} &= -\beta \frac{\theta}{T_0} g_i - \frac{1}{\rho_0} \frac{\partial p}{\partial x_i} + \nu \frac{\partial^2 u_i}{\partial x_j^2} \\ \frac{\partial \theta}{\partial t} + u_j \frac{\partial \theta}{x_j} &= \alpha \frac{\partial^2 \theta}{\partial x_j^2} \end{aligned} \tag{1}$$

, where $\beta$is the volumetric expansion coefficient, usually approximated as the reciprocal of the reference temperature $\beta = \frac{1}{T_0}$. α is the thermal diffusivity, defined as

$$\alpha = \frac{k}{\rho c_p}$$

. The dimensional number Rayleigh number Ra and Prandtl number Pr are defined as

$$Ra = \frac{\beta \Delta T g h^3}{\nu^2} Pr$$

$$Pr = \frac{c_p \mu}{k}$$

where g is the effect of the gravity.

The Nusselt number Nu is proportinal to the surface average of the temperature gradient of the top and bottom walls, written as

$$Nu = \frac{4a^2}{\pi} \int_0^{2\pi} \int_0^{\frac{1}{2a}} r \left(- \frac{\partial T}{\partial z}\bigg|_{z=0,h} \right) dr \, d\theta$$

The three-dimensional mesh of the cylindrical geometry is shown in Figure 2. At all the walls the shear-free velocity boundary condition is prescribed. The cylinder is evenly heated from below at a constant higher temperature $T_{bottom} = T_0 + \frac{\Delta T}{2}$and cooled from the top at a lower temperature $T_{top} = T_0 - \frac{\Delta T}{2}$. The temperatures are defined in such a way that the mean temperature equals the reference temperature of the Boussinesq model. The cylinder sidewall is assumed to be adiabatic. The mesh of the geometry has 36 cells in the radial direction and 32 cells on the vertical direction, such that the total element number approaches the mesh used by Neumann.

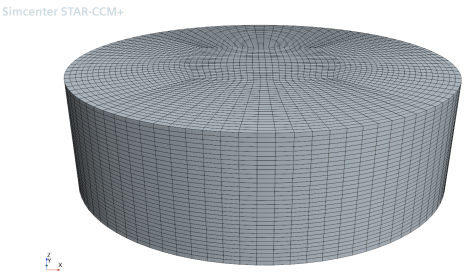

Figure 2: Mesh for the Neumann validation case, with L=36 cells on radial and N=32 on vertical direction

The simulation is performed iteratively by an implicit unsteady coupled solver using 2nd-order

temporal discretization with constant 0.01s timestep and bounded 3rd-order central differencing spacial discretization. A laminar flow regime is assumed. The numerical computation starts with an initial condition with zero-velocity and linearly-distributed temperature field. The whole system is operating under atmospheric pressure.

Physical meaning	Symbol	Value
aspect ratio	a	0.2899
thermal diffusivity	α	$1.8315 \times 10^{-5} m^2 s^{-1}$
volumetric expansion coefficient	β	$0.00333 K^{-1}$
specific heat	c_p	$1010.03 J kg^{-1} K^{-1}$
cylinder diameter	d	$0.0345 m$
gravity	g	$[0, 0, -9.81 m s^{-2}]$
thermal conductivity	k	$0.0217728 W m^{-1} K^{-1}$
dynamic viscosity	μ	$2.13154 \times 10^{-5} Pa\ s$
kinematic viscosity	ν	$1.81100 \times 10^{-5} m^2 s^1$
density	ρ	
pressure	p	
time	t	
temperature	T	
velocity	u	
spacial coordinate	x	

Table 1: List of symbols and values

2.2 Validation Results

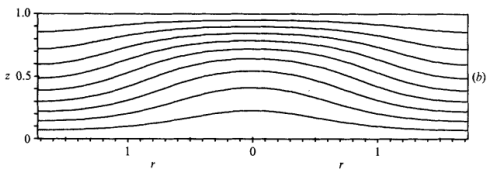

Figure 3: Isotherms from Neumann's paper with Ra=700 and Pr=1.

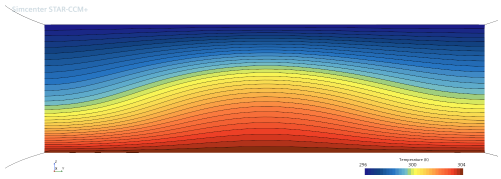

Figure 4: Isotherms from validation case with Ra=750 and Pr=1.

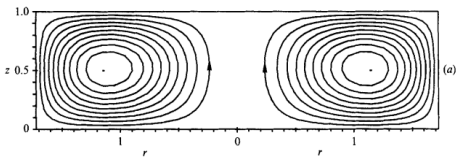

Figure 5: Streamlines from Neumann with Ra=700 and Pr=1.

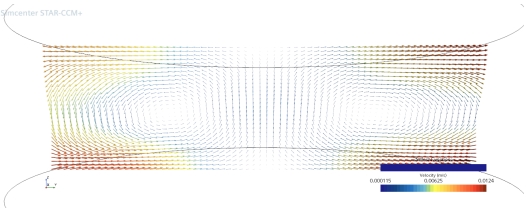

Figure 6: Streamlines from validation case

After residuals has been reduced by three orders of magnitude, the iteration is stopped. With $Pr = 1$, Figure and Figure show the isotherms from Neumann's work and the validation at Rayleigh number $Ra = 700$ and $Ra = 750$, respectively. It can be seen that the heat is concentrated in the center of the cylinder. Due to symmetry and adiabatic wall, the temperature gradient is zero at the center and the vertical sidewall. Figure and Figure indicate the modeled streamlines for Neumann's work and the velocity field of the the validation. The air rises from the cylinder center to the top and

returns from the sides to the bottom. The streamlines are circular and smooth, suggesting that the convection is laminar and steady.

add critical Ra number

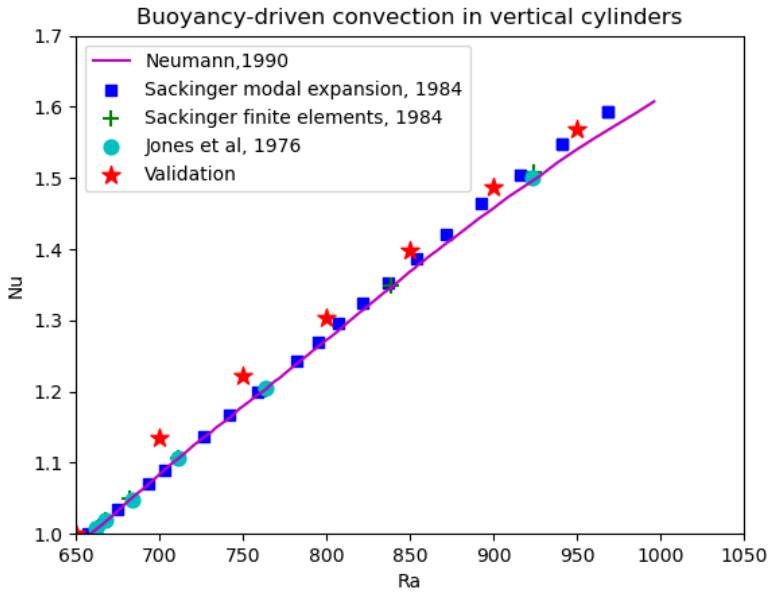

Figure 7: Nusselt number versus Rayleigh number for axisymmetric convection

The Nusselt numbers under different Rayleigh numbers are studied. Good agreement with the numerical results done by previous works (add three/ four refs here) is obtained.

The critical Rayleigh number $Ra_{c,s} = 657.51$ marks the onset of axisymmetric convection. Through the simulation it is observed that the modeled value of this number is sensitive to mesh, air properties, and discretization scheme. Figure 7 shows the comparison of different numerical method results. At $Ra = 650$ an unity Nusselt number is obtained, meaning that the convection is still not in effect. The heat is only transferred by thermal conduction. This could be verified by the perfectly stratified temperature distribution and the velocity vectors close to zero everywhere. At $Ra = 700$ an inclined temperature stratification, shown in Figure 8, and a one-roll velocity field 9 are obtained. These are different from Neumann's work, which sees the onset of axisymmetric convection. This could be a result of using the bounded 3rd-order central difference method, which adds more numerical diffusion to the solution. However, it is clear that the convection starts to be in effect when the Rayleigh number is larger than 650 and smaller than 700(or 750?), making the validation good.

When $Ra \geq 650$ the Nu number becomes larger than one and rises linearly with the Ra number, suggesting the onset of the natural convection in a laminar regime.

It is worth noticing that when $Ra \geq 700$ there is nuance between the validation and the numerical results. The reason could be a result of the $Pr = 1$ assumption that is widely adopted in the field of numerical fluid mechanics, while from an engineering perspective the Prandtl number of the real air under ambient temperature is around 0.71. Slight adjustment was make to approximate the Prantdl number to 1 thus viscosity and conductivity deviate from reality. However, the general trend of the Nusselt number versus Rayleigh number show good agreement with the previous numerical results.

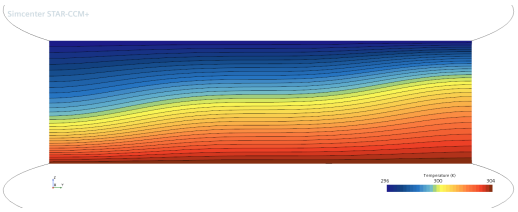

Figure 8: Isotherms from validation case with Ra=700 and Pr=1.

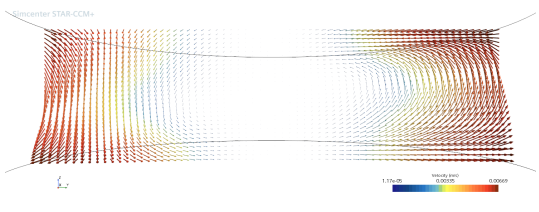

Figure 9: Velocity from validation case with Ra=700 and Pr=1.

3 Surge vessel with different Rayleigh numbers

3.1 Physical set-up

Large Eddy Simulation(LES) is used to model the flow and heat transfer inside the surge vessel. The three-dimensional model size is adopted in such a way that it matches with the measurement. During the measurement, the water is drained from ??? till the water lever reaches 1.75m below the first flanges. The simulation starts then when the water level is kept stationary until a new equilibrium is reached.

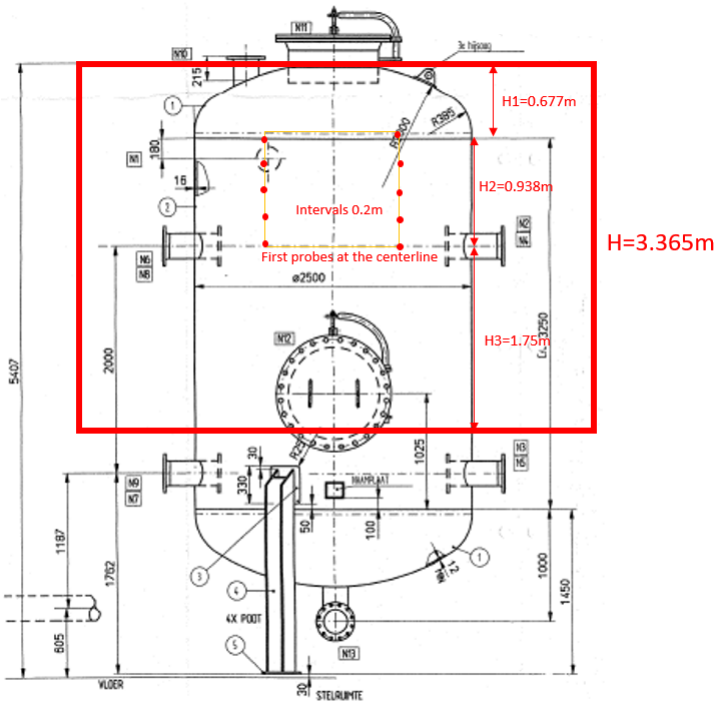

Figure 10: Schematic Diagram of the Blue Vessel

Figure 10 shows a schematic diagram of the adopted modeled size. The effect of the flanges and outlets is neglected in the physical model due to its minor in influence to the flow. The rounded-top of the vessel is approximated to be a cylinder top. Hence, a cylinder with 3.365m in height and 2.5m in diameter is used for the simulation. To better compare with the results from measurement, during which temperatures are measured using 20 probes located at center top of the vessel, with 20 K-type and 5 T-type. The probes are evenly placed on the vertical frames with the frame center at the vertical center line of the cylinder. The height level of the lowest probes are at the same level with the center line of the first flanges. The interval of each row of probes is 0.2m.

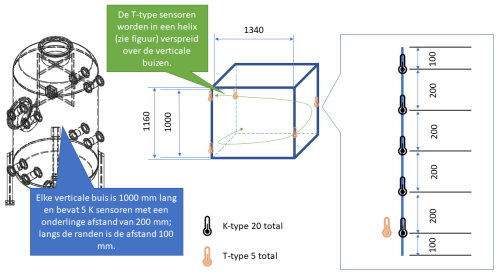

Figure 11: Schematic Diagram of the Probes Locations in the Measurement

Figure 12: A Picture of the Probes Locations in the Measurement

3.2 Numerical Model

To compare the air flow and heat transfer in different size of vessels. Two vessels under two different Rayleigh numbers are simulated. The low Ra one has the dimension of 1/10 of the vessel air cavity size, that is, a cylinder with $0.3365m$ in height and $0.25m$ in diameter, with Rayleigh number $Ra = 5.6 \times 10^7$. The high Rayleigh case takes the actual size of air volume, with height $h = 3.365m$, diameter $d = 2.5m$, and $Ra = 5.6 \times 10^{10}$.

The air is modeled through LES method. The WALE(Wall-Adapting Local-Eddy Viscosity) Subgrid Scale model is used in simulation given it advantages of being less sensitive to to value of the model coefficient and it automatically gives accurate scaling at walls. The subgrid scale viscosity is expressed as

$$\mu_t = \rho \Delta^2 S_W$$

where ρ is the density, Δ is the grid filter width, S_w is a deformation parameter.

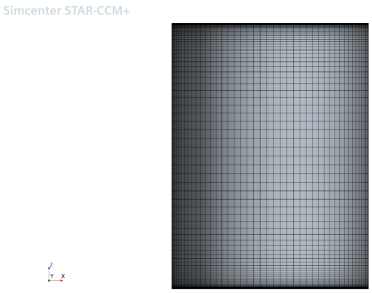

Figure 13: Mesh of the cylinder with low Ra: top view

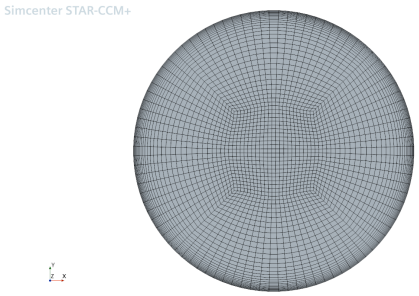

Figure 14: Mesh of the cylinder with low Ra: side view

Figure 14 and 13 show the side view and top view of the mesh for the low Rayleigh number used. The grids near all the boundaries are refined in such a way that the wall shear stress $y+$ values smaller than 1. The mesh for high Rayleigh number vessel is shown in Figure 15. O-block topology is utilized to generate the fine meshes, with all the cell quality above 0.7. The detailed values of the two meshes are listed in Table **??**.

The iteration starts with the initial air temperature at 273 K under atmospheric pressure. The air properties are listed in Table **??**. Isothermal at 288 K and no-slip boundary conditions at top, bottom, and sidewall are prescribed. Bounded Central-Differencing spatial discretization is applied for an implicit unsteady coupled solver with a blending factor 0.15 and time step 0.01s using 2st-order upwind temporal scheme. Incompressible ideal gas(also referred as Low Mach number Derivation) is

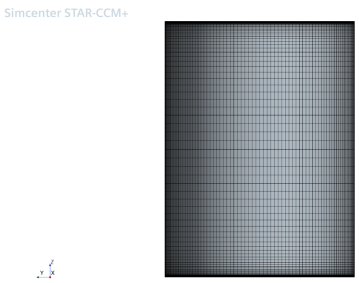

Figure 15: Mesh of the cylinder with high Ra: side view

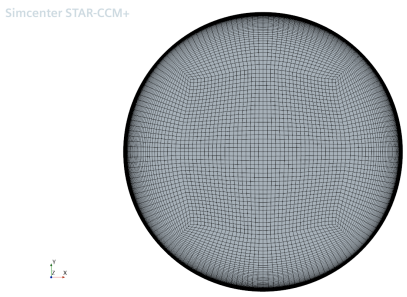

Figure 16: Mesh of the cylinder with high Ra: top view

Physical meaning	Symbol	Value
dynamic viscosity	μ	$1.759956^{-5} Pa \cdot s$
Molecular weight	M	$28.9664 kg/kmol$
Specific heat	c_p	$1006.76 J/kg \cdot K$
Thermal conductivity	k	$0.0249942 W/m \cdot K$
Turbulent Prandtl number	Prt	0.9

Table 2: Air properties

	$Ra = 5.6 \times 10^7$	$Ra = 5.6 \times 10^{10}$
height	$0.3655m$	$3.655m$
diameter	$0.25m$	$2.5m$
mesh number on radial direction	42	50
mesh number on vertical direction	80	120
element number	277242	1385928
wall spacing(top and bottom)	$0.0004m$	$0.0001m$
wall spacing(sidewall)	$0.0004m$	$0.0001m$
Max CFL number	0.933	1.021
Max CFL number	0.723	0.833

Table 3: Dimension of the meshes

used, written as follows:

$$\begin{aligned} \frac{\partial \rho}{\partial t} + \frac{\partial \rho u_j}{\partial x_j} &= 0, \\ \frac{\partial \rho u_i}{\partial t} + \frac{\partial \rho u_j u_i}{\partial x_j} + \frac{\partial P}{\partial x_j} &= \frac{\partial \tau_{ij}}{\partial x_j} + (\rho - \rho_0) g_i, \\ \frac{\partial \rho h}{\partial t} + \frac{\partial \rho u_j h}{\partial x_j} &= -\frac{\partial q_j}{\partial x_j} + \frac{P_{th}}{\partial t}, \end{aligned} \tag{2}$$

, where g_i is the gravity vector, h is the specific enthalpy, q_j is the heat conduction. Pressure is assumed as follows:

$$P_{th} = \rho \frac{R}{W} T$$

, where W is the mean molecular weight of the gas. τ is the viscous shear stress tensor, defined as

$$\tau_{ij} = \mu \left(\frac{\partial u_i}{\partial x_j} + \frac{\partial u_j}{\partial x_i} \right) - \frac{2}{3} \mu \frac{\partial u_k}{\partial x_k} \delta_{ij}$$

3.3 Results

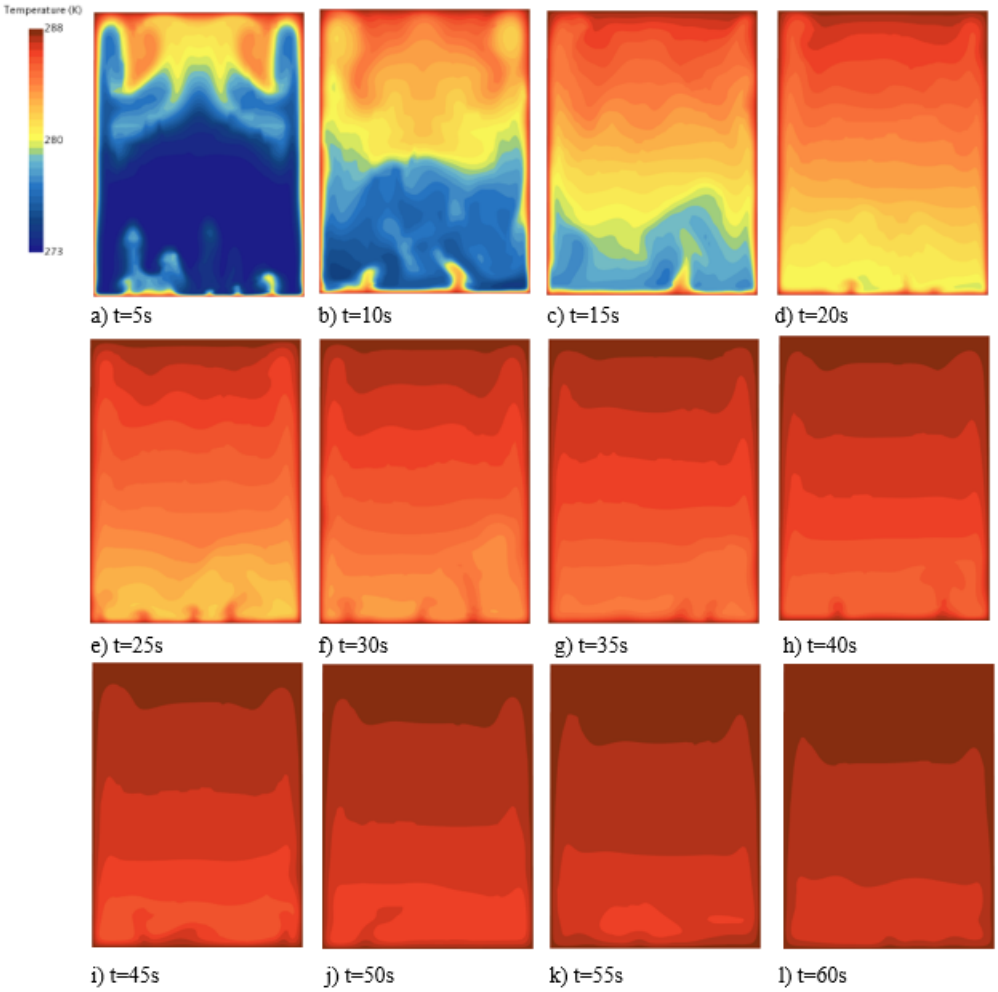

Figure 17: Temperature fields with $Ra = 5.6 \times 10^7$, time interval $\Delta t = 20s$.

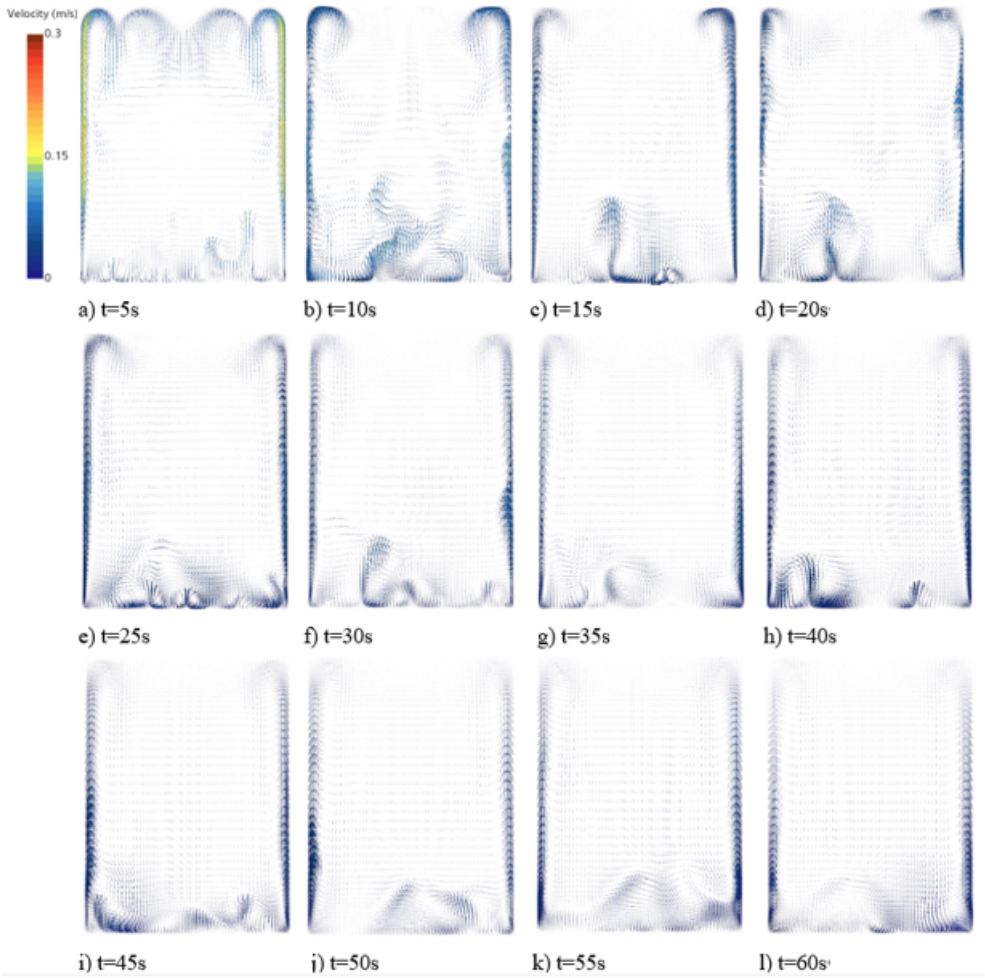

Figure 18: Velocity field with $Ra = 5.6 \times 10^7$, time interval $\Delta t = 20s$.

Figure 19 and Figure 20 show the residual of the simulation. The iterations are stopped when the residual is significantly reduced and sufficiently small.

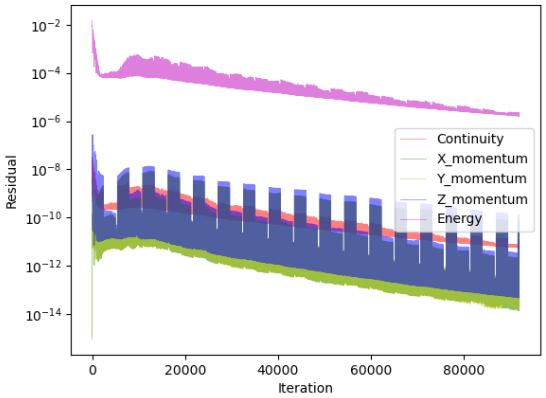

Figure 19: Residual $Ra = 5.6 \times 10^7$

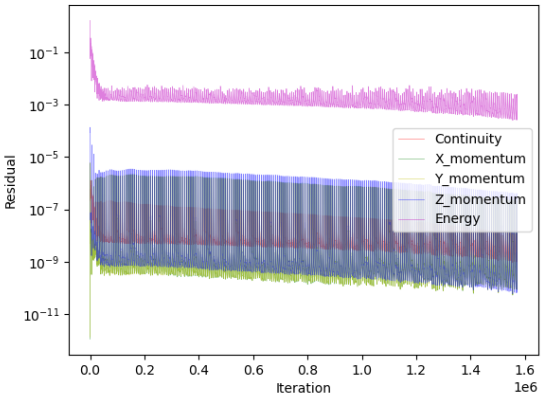

Figure 20: Residual $Ra = 5.6 \times 10^{10}$

Figure 17 and 18 show the temperature and velocity evolution with $Ra = 5.6 \times 10^7$. In the first 5s, driven by the temperature difference between the air and the wall, momentum and thermal boundary layers are formed at the sidewall bottom and grow thicker gradually along the vertical wall. The momentum boundary layer is well resolved by the fine mesh near the wall, as indicated in Figure 24 showing the velocity profile on a horizontal line passing the cylinder center at 0.7h height level.

The air near the sidewall is heated and rises to the top corner under the effect of gravity, resulting in a circular flow at the corner and a downward bulk plume at the center of the cylinder as mass is conserved. The flow near the sidewall appears laminar and symmetric within the first 5s but rapidly turns into turbulent afterwards. Air near the bottom is heated and forms small vortices. Vortices rises up and dissipates into the bulk air. This flow is turbulent as a result of the instability caused by the heating from below, during which the transition from laminar to turbulent happens at much lower Rayleigh number. The flow patterns here is similar with which could be observed in Rayleigh-Benard convection, while in this case the domain is also heated from far top.

After 5s, the rise of the air along the vertical wall and the consequencing circle flow and downward plume still exist, bringing the high temperature isotherms growing slowly downward. Because the temperature difference is becoming smaller at the vertical and top boundaries, the velocity of the upward flow at the sidewall and the downward flow at the center gradually slow down. A temperature stratification can be observed until the system gets infinitely close to 288K.

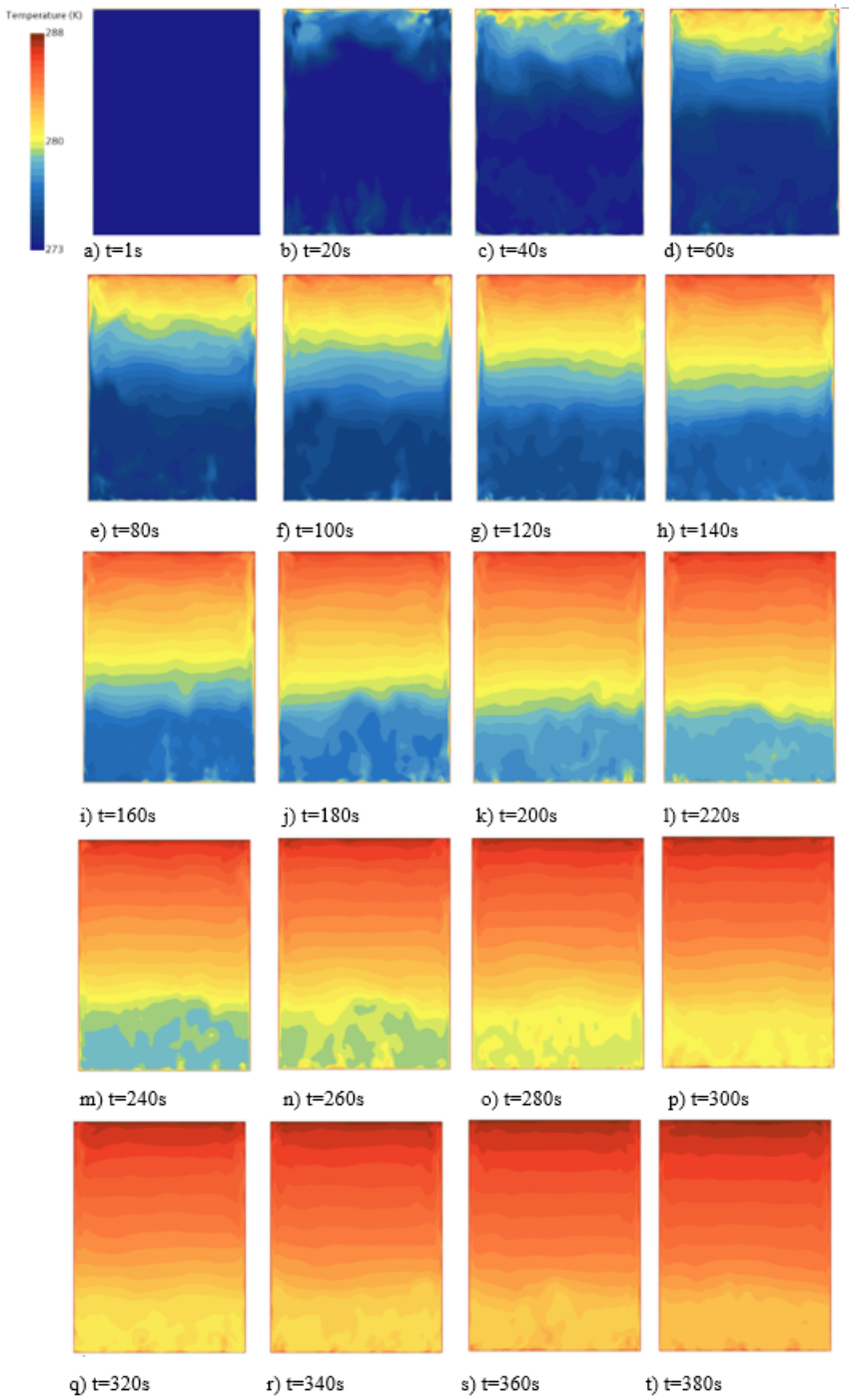

Figure 21: Temperature field with $Ra = 5.6 \times 10^{11}$ on the central vertical plane, time interval $\Delta t = 20s$.

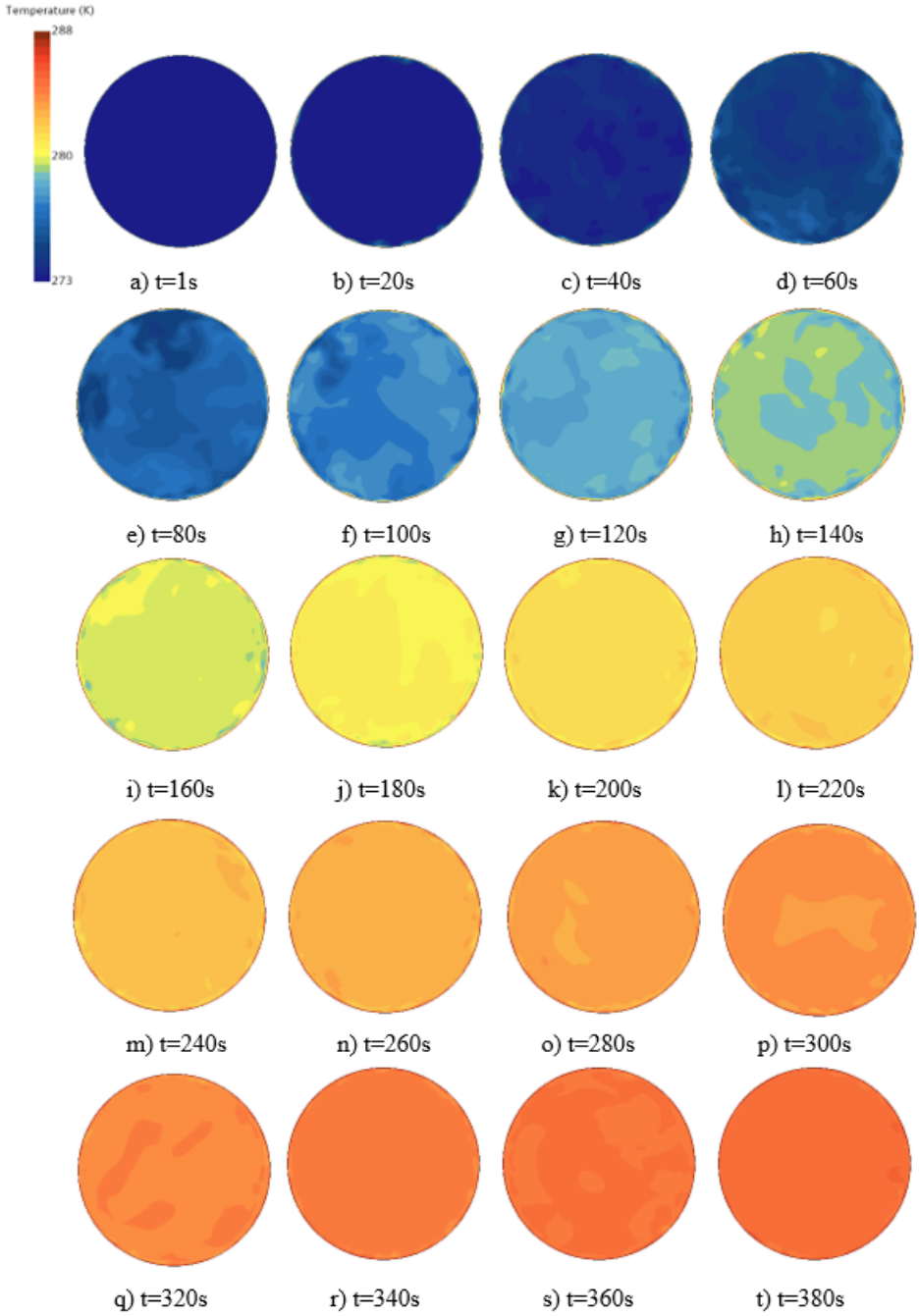

Figure 22: Temperature field with $Ra = 5.6 \times 10^{11}$ on the center horizontal plane, time interval $\Delta t = 20s$.

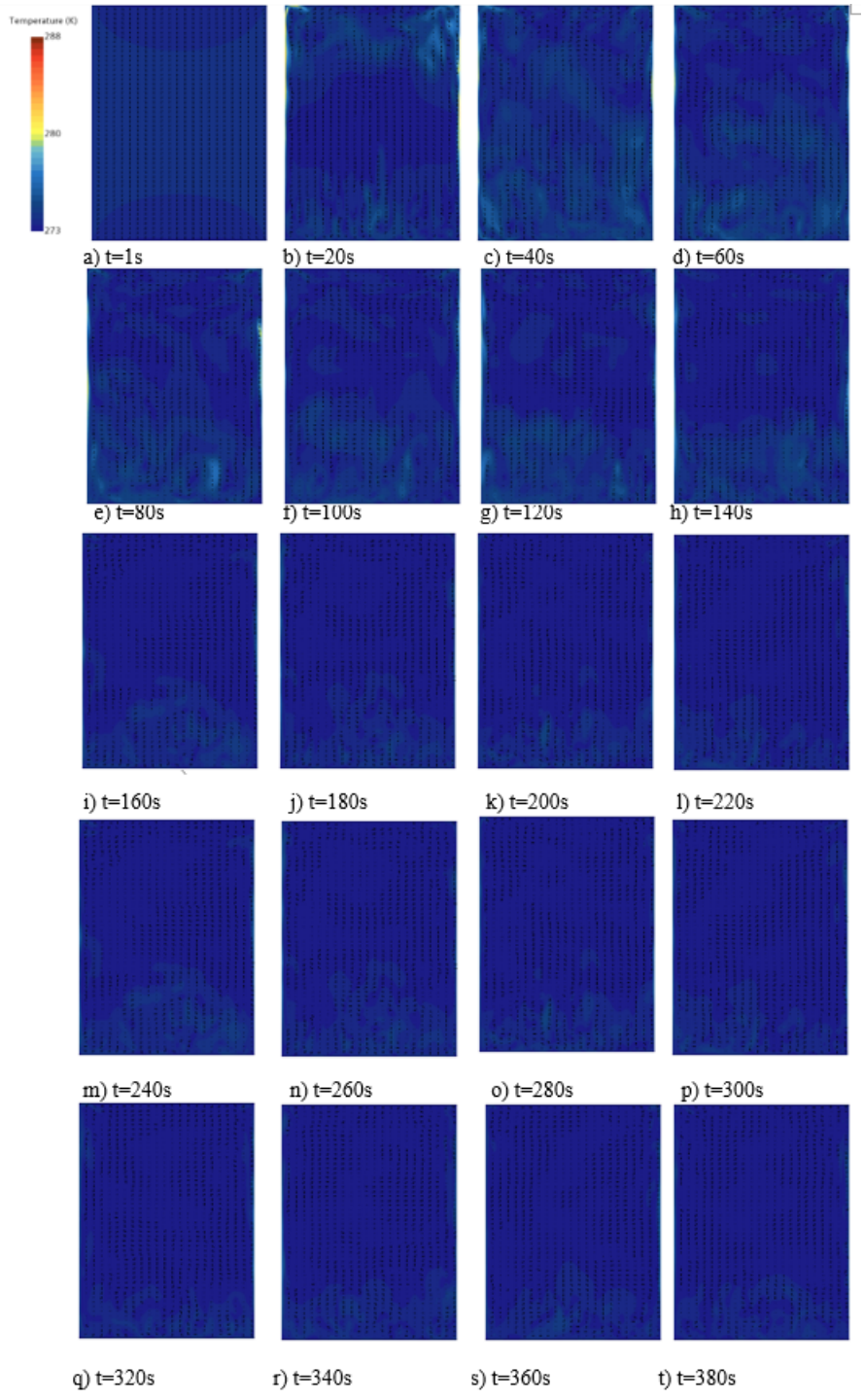

Figure 23: Velocity field with $Ra = 5.6 \times 10^{11}$, time interval $\Delta t = 20s$.

Figure 21 and Figure 22 indicate the temperature distribution evolution at the vertical center plane and horizontal center plane. Velocity fields are presented in Figure 23. The dimension of the $Ra = 5.6\times10^{11}$ is ten times of $Ra = 5.6\times10^{7}$ with the same initial conditions and boundary conditions. Similar with $Ra = 5.6 \times 10^{7}$, a well resolved thin boundary layer with its velocity profile shown in Figure 25, develops at the vertical cylinder wall, resulting in a circular flow pattern at the top corner. A clear temperature stratification evolution with time is presented in Figure 26. However, because of the much larger geometry and Rayleigh number, the flow gets turbulent faster and more intensively as the process starts. Hence, the downward plume at the center appears well-mixed and thus the temperature distributes more evenly than the flow with low Rayleigh number, as can be observed that the isotherms are flatter in each temperature layer. Several small upward plumes can be found within the vertical velocity boundary layer as it grows. It takes more than 400s for the mean temperature to converge to 288K, while 400s is sufficient to present the major heat transfer behaviors and flow patterns.

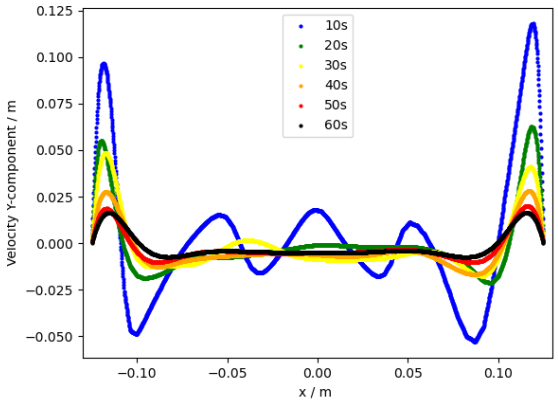

Figure 24: Velocity as a function of horizontal location at $0.7h$ height level, $Ra = 5.6 \times 10^{7}$

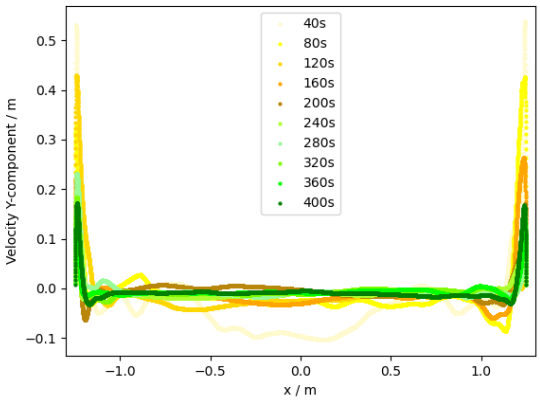

Figure 25: Velocity as a function of horizontal location at $0.7h$ height level, $Ra = 5.6 \times 10^{10}$

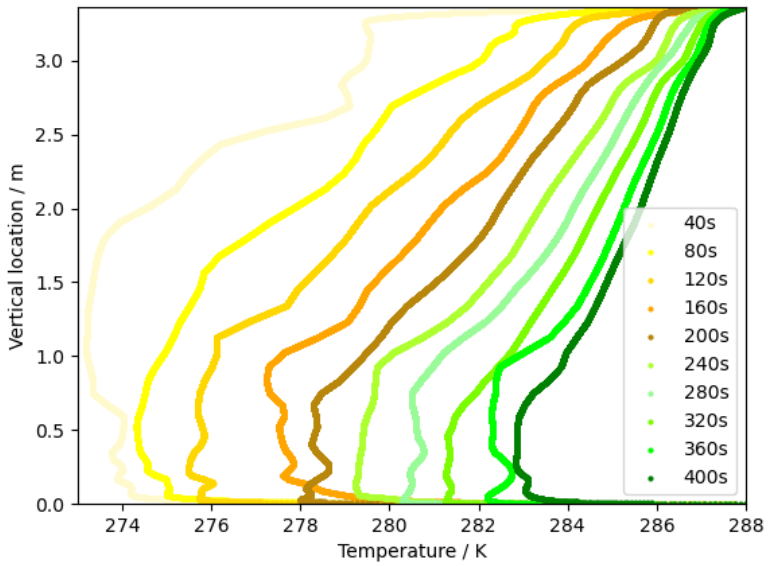

Figure 26: Temperatures as a function of vertical location at the cylinder centerline, $Ra = 5.6 \times 10^{10}$.

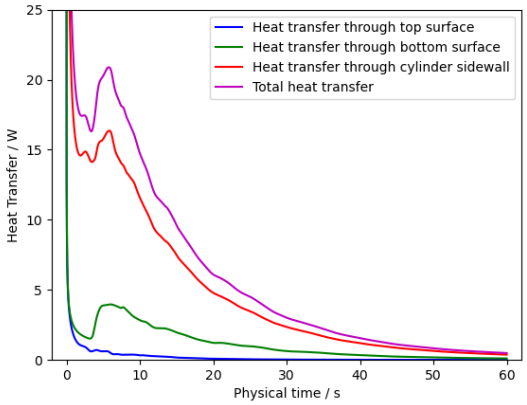

Figure 27: Heat Transfer through surfaces with $Ra = 5.6 \times 10^7$

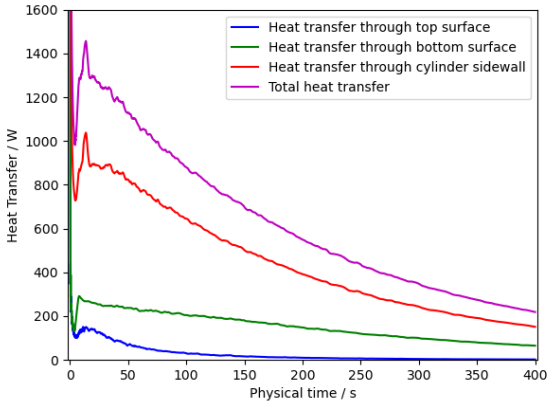

Figure 28: Heat Transfer through surfaces with $Ra = 5.6 \times 10^{10}$

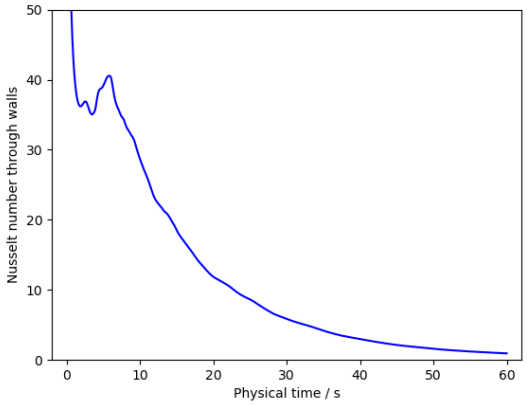

Figure 29: Nusselt number at surfaces with $Ra = 5.6 \times 10^7$.

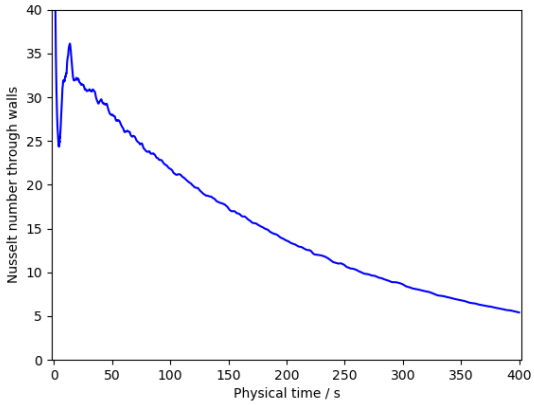

Figure 30: Nusselt number at surfaces with $Ra = 5.6 \times 10^{10}$.

Figure 27 and Figure 28 indicate the heat transfer through the walls. The results that showing the heat transfer is profound at the beginning is based on the assumption that the boundary has $\Delta T = 15°C$ without a prescribed boundary layer. Thus temperature gradient is large at first and decrease rapidly when the boundary layer is growing. Heat transferred through the sidewall is dominant during the whole process. In both cases, a heat transfer peak shows up a few seconds after the simulation is started at both vertical and bottom boundaries. This could be a result of the transition from laminar to turbulent flow regime, in which the energy is transferred more intensively. Then the temperature heat transfer rate decreases as the temperature difference decreases. Total Nusselt number on all surfaces are shown in Figure 29 and Figure 29. Since Nusselt number is defined as a function of the temperature gradient, the change of the Nusselt number show similar behavior with the total heat transfer curves, with a peak at the beginning representing the transition of the flow regime and the sidewall.

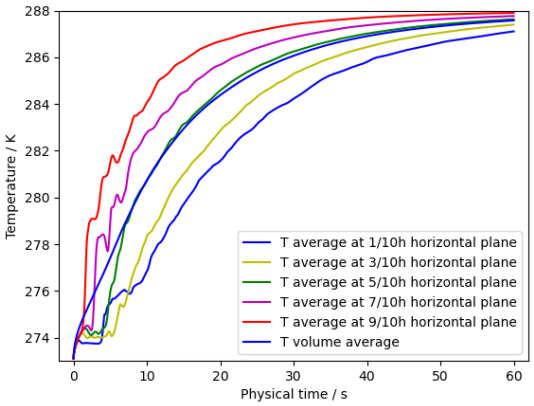

Figure 31: Average temperature of different planes with $Ra = 5.6 \times 10^7$.

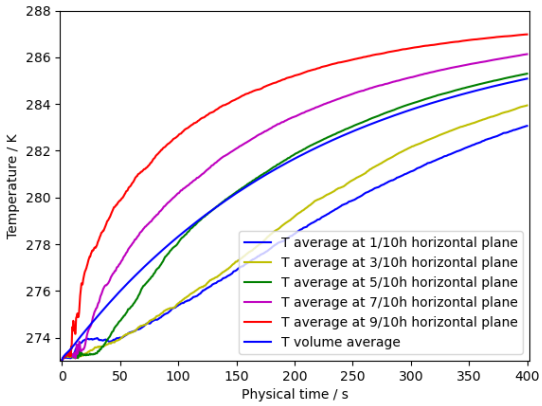

Figure 32: Average temperature of different planes with $Ra = 5.6 \times 10^{10}$.

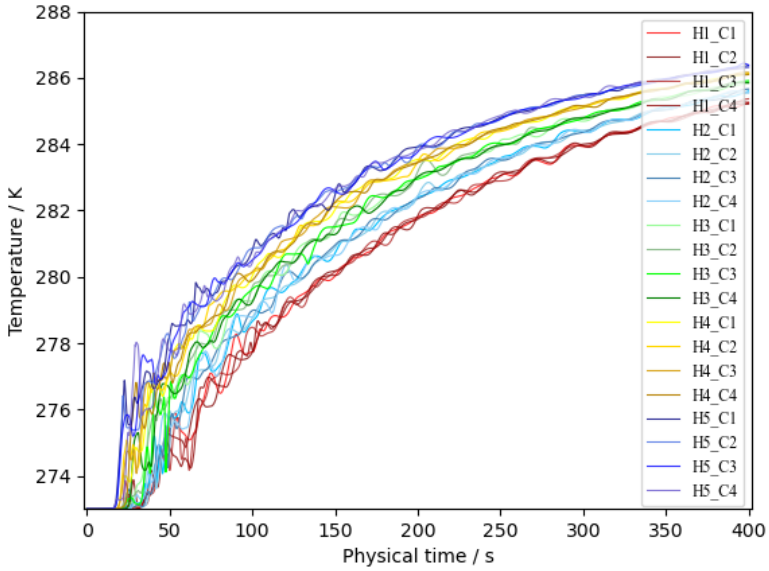

Figure 33: Temperatures at probes locations with $Ra = 5.6 \times 10^{10}$.

Figure 31 and Figure 32 show the averaged temperature on the horizontal planes of different heights. The virtual planes are at 0.1, 0.3, 0.5, 0.7, 0.9times the total height of the cylinder. The temperature at the top surface increases faster than that at the bottom. Figure 33 shows the simulated temperatures at the locations where the probes are beings placed, where H1 indicates the probes at the lowest height level and C indicates the horizontal location.

4 Conclusion

Include Mike's results find something to compare:

5 Appendix

5.1 Graph Appendix

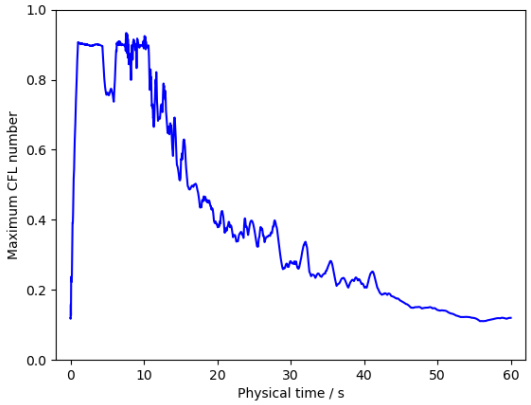

Figure A.1: Maximum CFL number with $Ra = 5.6 \times 10^7$.

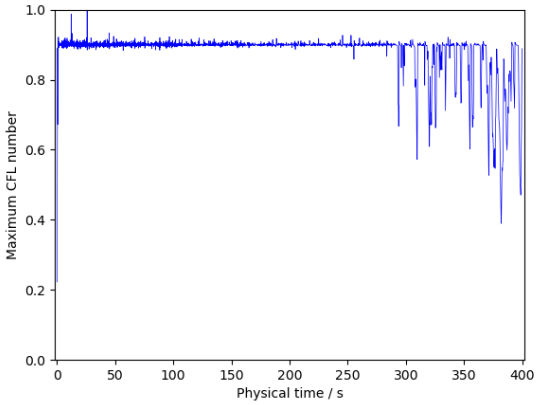

Figure A.2: Maximum CFL number with $Ra = 5.6 \times 10^{10}$.

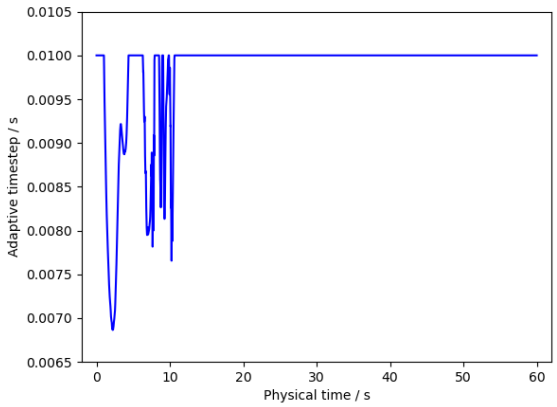

Figure A.3: Adaptive timestep with $Ra = 5.6 \times 10^7$

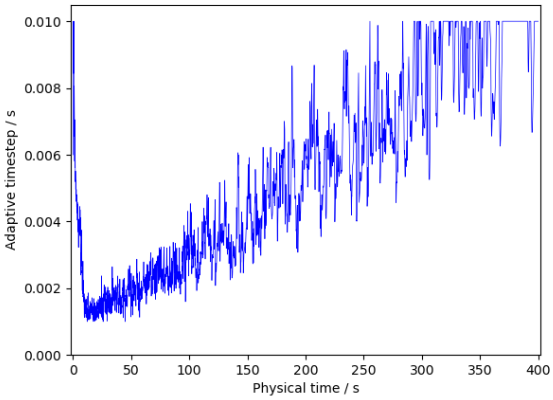

Figure A.4: Adaptive timestep with $Ra = 5.6 \times 10^{10}$.

Figure A.1 and Figure A.2 show the maximum CFL number that exists entire computation domain with respect to physical timescale. Figure A.1 and Figure A.2 suggest the corresponding timestep that is used. In order to facilitate the simulation, adaptive timestep method is applied in such a way that the mean CFL number is 0.7 and the maximum CFL number is controlled to be lower than 0.9. During the iteration with $Ra = 5.6 \times 10^7$, the CFL number is large at the beginning but drops significantly with time, while the adaptive timestep becomes 0.01s when the CFL number decreases. This could be a result of the assumption that the temperature difference becomes smaller, thus the buoyancy-driven velocity also becomes smaller, allowing each grid to use larger timestep under the condition that $CFL < 1$ is satisfied. However, 0.01s is the prescribed timestep of the implicit unsteady solver and the maximum timestep of the adaptive method. Since the timestep larger than 0.01s could be used, but the maximum timestep is limited, the CFL number would be decreased due to the reduction in the velocity. Similarly, for the vessel with $Ra = 5.6 \times 10^{10}$, the timestep gradually becomes larger as the iteration proceeds. But due to larger dimension and more complex turbulence, the timestep that can be automatically applied has not reached 0.01s yet.

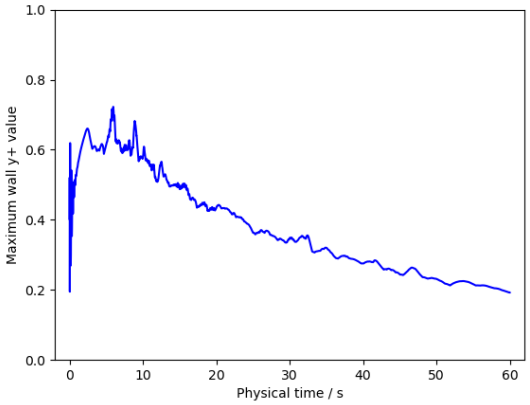

Figure A.5: Maximum wall $y+$ value with $Ra = 5.6 \times 10^7$.

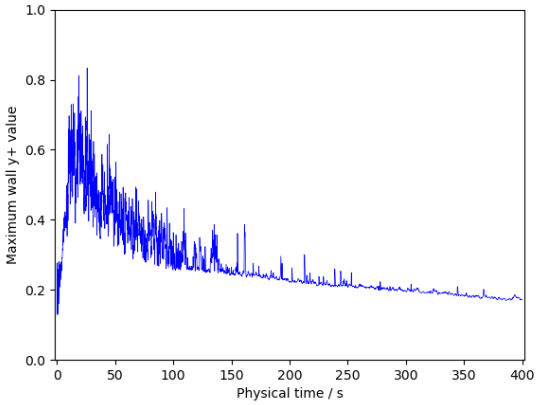

Figure A.6: Maximum wall $y+$ value with $Ra = 5.6 \times 10^{10}$.

The domain-maximum wall $y+$ vales are shown in A.5 and Figure A.5. By having small cell spacing at the walls, the $y+$ vales are smaller than 1, meaning that the boundary layers are well-resolved.

References

[1] S van der Zwan, M Toussaint, A Alidai, IWM Pothof, and PH Leruth. Thermodynamics of surge vessels. In *BHR Group*, 2015.

[2] HR Graze. A rational thermodynamic equation for air chamber design. In *3rd Australasian Conf. on Hydraulics and Fluid Mechanics*, pages 57–61, 1968.

[3] S Van der Zwan, D Rudolph, SH Balkema, IWM Pothof, and PH Leruth. Optimization of surge protection for a large water transmission scheme in abu dhabi. In *11th international conference on pressure surges, Lisbon, Portugal*, pages 1–11. BHR Group Ltd., 2012.

[4] G Neumann. Three-dimensional numerical simulation of buoyancy-driven convection in vertical cylinders heated from below. *Journal of Fluid Mechanics*, 214:559–578, 1990.

[5] S Chandrasekhar Hydrodynamic. hydromagnetic stability oxford university press, 1961.

[6] Roshan Samuel, Ravi Samtaney, and Mahendra K Verma. Large-eddy simulation of rayleigh-b\'enard convection for extreme rayleigh numbers. *arXiv preprint arXiv:2204.03697*, 2022.

[7] LB Evans, RC Reid, and EM Drake. Transient natural convection in a vertical cylinder. *AIChE Journal*, 14(2):251–259, 1968.

[8] E Papanicolaou and V Belessiotis. Transient natural convection in a cylindrical enclosure at high rayleigh numbers. *International Journal of Heat and Mass Transfer*, 45(7):1425–1444, 2002.

[9] S-H Peng, K Hanjalic, and Lars Davidson. Large-eddy simulation and deduced scaling analysis of rayleigh–bénard convection up to ra= 109. *Journal of Turbulence*, (7):N66, 2006.

5.2 Python Code

Code 1: Cpplot.py

```
%copy and paste code here

\clearpage
\begin{figure}[h]
    \centering
    \subfigure {
    \includegraphics[width=1.2cm]{Figs/T_low_Ra_colorbar.png}
    }
    \subfigure a){
    \includegraphics[width=2.7cm]{Figs/Low_Ra_5ss_T.png}
    }
    \subfigure b){
    \includegraphics[width=2.7cm]{Figs/Low_Ra_10ss_T.png}
    }
    \subfigure c){
    \includegraphics[width=2.7cm]{Figs/Low_Ra_15ss_T.png}
    }
    \subfigure d){
    \includegraphics[width=2.7cm]{Figs/Low_Ra_20ss_T.png}
    }
    \quad   \\
    \quad
    \subfigure e){
    \includegraphics[width=2.7cm]{Figs/Low_Ra_25ss_T.png}
    }
    \subfigure f){
    \includegraphics[width=2.7cm]{Figs/Low_Ra_30ss_T.png}
    }
    \subfigure g){
    \includegraphics[width=2.7cm]{Figs/Low_Ra_35ss_T.png}
    }
    \subfigure h){
    \includegraphics[width=2.7cm]{Figs/Low_Ra_40ss_T.png}
    }
    \quad   \\
    \quad
    \subfigure h){
    \includegraphics[width=2.7cm]{Figs/Low_Ra_45ss_T.png}
    }
    \subfigure i){
    \includegraphics[width=2.7cm]{Figs/Low_Ra_50ss_T.png}
    }
    \subfigure j){
    \includegraphics[width=2.7cm]{Figs/Low_Ra_55ss_T.png}
    }
    \subfigure k){
    \includegraphics[width=2.7cm]{Figs/Low_Ra_60ss_T.png}
    }
    \quad   \\

    \caption{Temperature fields with $Ra=5.6 \times 10^7 $,,time interval $\Delta t=20s$.}
    \label{T_panal_low_Ra}
\end{figure}

\begin{figure}[h]
    \centering
    \subfigure {
```

```
    \includegraphics[width=1.0cm]{Figs/Low_Ra_colorbar_V.png}
    }
    \subfigure a){
    \includegraphics[width=2.7cm]{Figs/Low_Ra_5ss_V.png}
    }
    \subfigure b){
    \includegraphics[width=2.7cm]{Figs/Low_Ra_10ss_V.png}
    }
    \subfigure c){
    \includegraphics[width=2.7cm]{Figs/Low_Ra_15ss_V.png}
    }
    \subfigure d){
    \includegraphics[width=2.7cm]{Figs/Low_Ra_20ss_V.png}
    }
    \quad   \\
    \quad
    \subfigure e){
    \includegraphics[width=2.7cm]{Figs/Low_Ra_25ss_V.png}
    }
    \subfigure f){
    \includegraphics[width=2.7cm]{Figs/Low_Ra_30ss_V.png}
    }
    \subfigure g){
    \includegraphics[width=2.7cm]{Figs/Low_Ra_35ss_V.png}
    }
    \subfigure h){
    \includegraphics[width=2.7cm]{Figs/Low_Ra_40ss_V.png}
    }
    \quad   \\
    \quad
    \subfigure h){
    \includegraphics[width=2.7cm]{Figs/Low_Ra_45ss_V.png}
    }
    \subfigure i){
    \includegraphics[width=2.7cm]{Figs/Low_Ra_50ss_V.png}
    }
    \subfigure j){
    \includegraphics[width=2.7cm]{Figs/Low_Ra_55ss_V.png}
    }
    \subfigure k){
    \includegraphics[width=2.7cm]{Figs/Low_Ra_60ss_V.png}
    }
    \quad   \\

    \caption{Velocity field with $Ra=5.6 \times 10^7 $, time interval $\Delta t=20s$.}
    \label{V_panal_low_Ra}
\end{figure}

\begin{figure}[h]
    \centering
    \subfigure {
    \includegraphics[width=1.0cm]{Figs/T_low_Ra_colorbar.png}
    }
    \subfigure a){
    \includegraphics[width=2.7cm]{High_Ra_T&V_pics/T_ver_high_Ra_1ss.png}
    }
    \subfigure b){
    \includegraphics[width=2.7cm]{High_Ra_T&V_pics/T_ver_high_Ra_20ss.png}
    }
    \subfigure c){
    \includegraphics[width=2.7cm]{High_Ra_T&V_pics/T_ver_high_Ra_40ss.png}
```

```
}
\subfigure d){
\includegraphics[width=2.7cm]{High_Ra_T&V_pics/T_ver_high_Ra_60ss.png}
}
\quad   \\
\quad
\subfigure e){
\includegraphics[width=2.7cm]{High_Ra_T&V_pics/T_ver_high_Ra_80ss.png}
}
\subfigure f){
\includegraphics[width=2.7cm]{High_Ra_T&V_pics/T_ver_high_Ra_100ss.png}
}
\subfigure g){
\includegraphics[width=2.7cm]{High_Ra_T&V_pics/T_ver_high_Ra_120ss.png}
}
\subfigure h){
\includegraphics[width=2.7cm]{High_Ra_T&V_pics/T_ver_high_Ra_140ss.png}
}
\quad   \\
\quad
\subfigure i){
\includegraphics[width=2.7cm]{High_Ra_T&V_pics/T_ver_high_Ra_160ss.png}
}
\subfigure j){
\includegraphics[width=2.7cm]{High_Ra_T&V_pics/T_ver_high_Ra_180ss.png}
}
\subfigure k){
\includegraphics[width=2.7cm]{High_Ra_T&V_pics/T_ver_high_Ra_200ss.png}
}
\subfigure l){
\includegraphics[width=2.7cm]{High_Ra_T&V_pics/T_ver_high_Ra_220ss.png}
}
\quad   \\
\quad
\subfigure m){
\includegraphics[width=2.7cm]{High_Ra_T&V_pics/T_ver_high_Ra_240ss.png}
}
\subfigure n){
\includegraphics[width=2.7cm]{High_Ra_T&V_pics/T_ver_high_Ra_260ss.png}
}
\subfigure o){
\includegraphics[width=2.7cm]{High_Ra_T&V_pics/T_ver_high_Ra_280ss.png}
}
\subfigure p){
\includegraphics[width=2.7cm]{High_Ra_T&V_pics/T_ver_high_Ra_300ss.png}
}
\quad   \\
\quad
\subfigure h){
\includegraphics[width=2.7cm]{High_Ra_T&V_pics/T_ver_high_Ra_320ss.png}
}
\subfigure i){
\includegraphics[width=2.7cm]{High_Ra_T&V_pics/T_ver_high_Ra_340ss.png}
}
\subfigure j){
\includegraphics[width=2.7cm]{High_Ra_T&V_pics/T_ver_high_Ra_360ss.png}
}
\subfigure k){
\includegraphics[width=2.7cm]{High_Ra_T&V_pics/T_ver_high_Ra_380ss.png}
}
\quad   \\
```

```
    \caption{Temperature field with $Ra=5.6 \times 10^{11} $ on the central vertical plane, time inte
    \label{T_panal_high_Ra}
\end{figure}

\clearpage
\begin{figure}[h]
    \centering
    \subfigure {
    \includegraphics[width=1.0cm]{Figs/T_low_Ra_colorbar.png}
    }
    \subfigure a){
    \includegraphics[width=2.7cm]{High_Ra_T&V_pics/T_hor_high_Ra_1s.png}
    }
    \subfigure b){
    \includegraphics[width=2.7cm]{High_Ra_T&V_pics/T_hor_high_Ra_20s.png}
    }
    \subfigure c){
    \includegraphics[width=2.7cm]{High_Ra_T&V_pics/T_hor_high_Ra_40s.png}
    }
    \subfigure d){
    \includegraphics[width=2.7cm]{High_Ra_T&V_pics/T_hor_high_Ra_60s.png}
    }
    \quad   \\
    \quad
    \subfigure e){
    \includegraphics[width=2.7cm]{High_Ra_T&V_pics/T_hor_high_Ra_80s.png}
    }
    \subfigure f){
    \includegraphics[width=2.7cm]{High_Ra_T&V_pics/T_hor_high_Ra_100s.png}
    }
    \subfigure g){
    \includegraphics[width=2.7cm]{High_Ra_T&V_pics/T_hor_high_Ra_120s.png}
    }
    \subfigure h){
    \includegraphics[width=2.7cm]{High_Ra_T&V_pics/T_hor_high_Ra_140s.png}
    }
    \quad   \\
    \quad
    \subfigure i){
    \includegraphics[width=2.7cm]{High_Ra_T&V_pics/T_hor_high_Ra_160s.png}
    }
    \subfigure j){
    \includegraphics[width=2.7cm]{High_Ra_T&V_pics/T_hor_high_Ra_180s.png}
    }
    \subfigure k){
    \includegraphics[width=2.7cm]{High_Ra_T&V_pics/T_hor_high_Ra_200s.png}
    }
    \subfigure l){
    \includegraphics[width=2.7cm]{High_Ra_T&V_pics/T_hor_high_Ra_220s.png}
    }
    \quad   \\
    \quad
    \subfigure m){
    \includegraphics[width=2.7cm]{High_Ra_T&V_pics/T_hor_high_Ra_240s.png}
    }
    \subfigure n){
    \includegraphics[width=2.7cm]{High_Ra_T&V_pics/T_hor_high_Ra_260s.png}
    }
    \subfigure o){
    \includegraphics[width=2.7cm]{High_Ra_T&V_pics/T_hor_high_Ra_280s.png}
```

```
    }
    \subfigure p){
    \includegraphics[width=2.7cm]{High_Ra_T&V_pics/T_hor_high_Ra_300s.png}
    }
    \quad   \\
    \quad
    \subfigure h){
    \includegraphics[width=2.7cm]{High_Ra_T&V_pics/T_hor_high_Ra_320s.png}
    }
    \subfigure i){
    \includegraphics[width=2.7cm]{High_Ra_T&V_pics/T_hor_high_Ra_340s.png}
    }
    \subfigure j){
    \includegraphics[width=2.7cm]{High_Ra_T&V_pics/T_hor_high_Ra_360s.png}
    }
    \subfigure k){
    \includegraphics[width=2.7cm]{High_Ra_T&V_pics/T_hor_high_Ra_380s.png}
    }
    \quad   \\

    \caption{Temperature field with $Ra=5.6 \times 10^{11} $ on the center horizontal plane, time int
    \label{T_panal_hor_0.5}
\end{figure}

\clearpage
\begin{figure}[h]
    \centering
    \subfigure {
    \includegraphics[width=1.0cm]{High_Ra_T&V_pics/V_colarbar_high_Ra.png}
    }
    \subfigure a){
    \includegraphics[width=2.7cm]{High_Ra_T&V_pics/V_ver_high_Ra_1s.png}
    }
    \subfigure b){
    \includegraphics[width=2.7cm]{High_Ra_T&V_pics/V_ver_high_Ra_20s.png}
    }
    \subfigure c){
    \includegraphics[width=2.7cm]{High_Ra_T&V_pics/V_ver_high_Ra_40s.png}
    }
    \subfigure d){
    \includegraphics[width=2.7cm]{High_Ra_T&V_pics/V_ver_high_Ra_60s.png}
    }
    \quad   \\
    \quad
    \subfigure e){
    \includegraphics[width=2.7cm]{High_Ra_T&V_pics/V_ver_high_Ra_80s.png}
    }
    \subfigure f){
    \includegraphics[width=2.7cm]{High_Ra_T&V_pics/V_ver_high_Ra_100s.png}
    }
    \subfigure g){
    \includegraphics[width=2.7cm]{High_Ra_T&V_pics/V_ver_high_Ra_120s.png}
    }
    \subfigure h){
    \includegraphics[width=2.7cm]{High_Ra_T&V_pics/V_ver_high_Ra_140s.png}
    }
    \quad   \\
    \quad
    \subfigure i){
    \includegraphics[width=2.7cm]{High_Ra_T&V_pics/V_ver_high_Ra_160s.png}
    }
```

```
    \subfigure j){
    \includegraphics[width=2.7cm]{High_Ra_T&V_pics/V_ver_high_Ra_180s.png}
    }
    \subfigure k){
    \includegraphics[width=2.7cm]{High_Ra_T&V_pics/V_ver_high_Ra_200s.png}
    }
    \subfigure l){
    \includegraphics[width=2.7cm]{High_Ra_T&V_pics/V_ver_high_Ra_220s.png}
    }
    \quad   \\
    \quad
    \subfigure m){
    \includegraphics[width=2.7cm]{High_Ra_T&V_pics/V_ver_high_Ra_240s.png}
    }
    \subfigure n){
    \includegraphics[width=2.7cm]{High_Ra_T&V_pics/V_ver_high_Ra_260s.png}
    }
    \subfigure o){
    \includegraphics[width=2.7cm]{High_Ra_T&V_pics/V_ver_high_Ra_280s.png}
    }
    \subfigure p){
    \includegraphics[width=2.7cm]{High_Ra_T&V_pics/V_ver_high_Ra_300s.png}
    }
    \quad   \\
    \quad
    \subfigure h){
    \includegraphics[width=2.7cm]{High_Ra_T&V_pics/V_ver_high_Ra_320s.png}
    }
    \subfigure i){
    \includegraphics[width=2.7cm]{High_Ra_T&V_pics/V_ver_high_Ra_340s.png}
    }
    \subfigure j){
    \includegraphics[width=2.7cm]{High_Ra_T&V_pics/V_ver_high_Ra_360s.png}
    }
    \subfigure k){
    \includegraphics[width=2.7cm]{High_Ra_T&V_pics/V_ver_high_Ra_380s.png}
    }
    \quad   \\

    \caption{Evolution of velocity field with $Ra=5.6 \times 10^{11} $, time interval $\Delta t=20s$.
    \label{V_ver_panal_high_Ra}
\end{figure}
```